Dynamics of Atomic Stick-Slip Friction Examined with Atomic Force Microscopy and Atomistic Simulations at Overlapping Speeds

Xin-Z. Liu, Zhijiang Ye, Yalin Dong, Philip Egberts, Robert W. Carpick, and Ashlie Martini

Phys. Rev. Lett. **114**, 146102 — Published 6 April 2015

DOI: 10.1103/PhysRevLett.114.146102

Dynamics of atomic stick-slip friction examined with atomic force microscopy and atomistic simulations at overlapping speeds

Xin-Z. Liu[1,†], Zhijiang Ye[2,†], Yalin Dong[4], Philip Egberts[3], Robert W. Carpick[1], Ashlie Martini[2]

[1]*Mechanical Engineering and Applied Mechanics, University of Pennsylvania, 220 S. 33rd Street, Philadelphia, PA, 19104 USA*

[2]*School of Engineering, University of California Merced, 5200 North Lake Road, Merced, California 95343 USA*

[3]*Department of Mechanical and Manufacturing Engineering, University of Calgary, 40 Research Place NW, Calgary, Alberta T2L 1Y6 Canada*

[4]*Department of Mechanical Engineering, University of Akron, 302 Buchtel Common, Akron, Ohio, 4325 USA*

[†]These authors contributed equally

Date: March 9, 2015

Abstract:

Atomic force microscopy (AFM) and atomistic simulations of atomic friction with silicon oxide tips sliding on Au(111) are conducted at overlapping speeds. Experimental data unambiguously reveals a stick-slip friction plateau above a critical scanning speed, in agreement with the thermally-activated Prandtl-Tomlinson (PTT) model. However, friction in experiments is larger than in simulations. PTT energetic parameters for the two are comparable, with minor differences due to contact area's influence on the barrier to slip. Recognizing that attempt frequency may be due to thermal vibrations of the larger AFM tip mass or instrument noise fully resolves the discrepancy. Thus, atomic stick-slip is well described by the PTT model if sources of slip-assisting energy are accounted for.

Atomic stick-slip sliding is an intriguing and fundamentally significant phenomenon, relevant to the understanding of elementary mechanisms of friction [1-3]. First observed using atomic force microscopy (AFM), atomic stick-slip often occurs when two clean surfaces, at least one of which is crystalline, slide in relative motion [4]. Reduced-order models, such as the Prandtl-Tomlinson (PT) model, reproduce a remarkable number of features of atomic stick-slip sliding [5,6]. These models explain the process as the build-up and then unstable release of energy in sufficiently compliant elastic elements of the system while traversing a periodic energy landscape (corresponding to the surface lattice sites) with sufficiently deep local energy minima. Upon slip at the maximum lateral force (the static friction force), physically unspecified

dissipation causes the interface to stop slipping at the next lattice site (or sometimes multiples thereof [7]) and the process repeats.

The PT model has recently been extended to include thermal energy, referred to as the PTT model, leading to the prediction that static friction will increase with decreasing temperature and increasing scanning speed (the speed at which the sample is translated with respect to the fixed end of the cantilever). The speed dependence of friction has been studied using AFM [8-13], but in only one case [8] was stick-slip behavior resolved. Although not all findings from those reports agree with each other, the trend of increasing friction as a function of velocity is explained as thermal energy assisting in overcoming local energy barriers: faster scanning reduces the time in which thermal energy has to provide this assistance and so static friction is higher. However, validating models quantitatively, understanding how energy is dissipated, and describing the atomic-level processes by which slip occurs dynamically at the interface are beyond the capabilities of the PTT model and are challenging because of the inaccessibility of the buried interface in experiments. Therefore, stick-slip is often considered using molecular dynamics (MD) simulations, which provides a means of directly observing atomic interactions within the interface [14,15]. However, the scanning speeds of AFM and MD have yet to overlap. This issue results from: (a) the femtosecond time steps used in standard MD to capture atomic motion which limit the time duration that can be simulated, constraining the simulations to high scanning speeds ($>10^{-1}$ m/s); and (b) the far slower scanning speeds ($<10^{-5}$ m/s) of AFM experiments which are typically constrained by mechanical and data acquisition limits. This discrepancy limits the ability to reliably compare results from AFM and MD.

Here, the gap between experiments and simulations was closed for the first time by using parallel replica dynamics (PRD) to slow down MD simulation scanning speeds, and by improving the AFM apparatus to obtain higher experimental scanning speeds, while resolving stick-slip behavior in both. Other parameters, namely environment (vacuum), materials (a gold sample and a SiO_2 tip), contact area, temperature, normal and lateral stiffnesses, and load, were also matched as closely as possible. Single stick-slip events were observed across 10 orders of magnitude of speed. However, the mean friction force at the same scanning speed was consistently higher in experiments than in simulations, and the trends fit to the thermally activated PTT model do not overlap. To identify sources of the discrepancy, the measured and

predicted friction trends were analyzed by comparing the corresponding physical parameters in the PTT model.

Experiments were conducted in an ultra-high vacuum (UHV) AFM (RHK 750, RHK Technology Inc.) at room temperature and a pressure of ~6×10^{-10} Torr. Gold samples were prepared by thermal evaporation of bulk gold onto freshly cleaved muscovite mica [16], flame annealed in air to produce (111) terraces, inserted in the fast entry lock of the UHV system, and subsequently baked at 160 °C for 8 hours before insertion into the main UHV AFM chamber. The cleanliness and the quality of the surface were confirmed by observing the Au(111) herringbone reconstruction on atomically-flat terraces (Figure S-1 in the Supplemental Material (SM) [17]). Due to the reconstruction, the Au(111) surface exhibits a periodic transition between face-centered cubic (FCC) and hexagonal close packed (HCP) crystallographic arrangements. Although there is some variation in friction between the two structures [26], only FCC areas were examined in this manuscript. Modifications to allow high speed stick-slip measurements are detailed in the SM [17]; the main innovations were the use of a compact shear piezo under the sample for fast lateral motion, and the implementation of high speed data acquisition electronics. Two different silicon contact-mode probes (Mikromash CSC 38, Mikromash Inc.) were used (called Tips 1 and 2 subsequently). Transmission electron microscopy (TEM) imaging confirmed the tips to be terminated in amorphous silicon oxide. The cantilevers were calibrated using the beam geometry method [27]. Friction signals were converted to forces using the procedure described in Ref. [28]. All data was acquired at an applied load of 0.0±0.2 nN in the presence of adhesion forces of 7.9±1.1 nN and 2.6±0.4 nN, for Tips 1 and 2, respectively. Both tips were scanned along the [110] direction of the Au(111) surface. The scan rate was varied randomly with ten cycles per scanning speed.

Pull-off force measurements provided a work of adhesion of 0.05±0.03 J/m^2 (averaged from 25 measurements). This value was used with the Derjaguin-Müller-Toporov (DMT) contact mechanics model [29] to estimate the tip radii to be 27±19 nm for Tip 1 and 8.6±5.8 nm for Tip 2 (details in SM [17]). For Tip 1, this value was consistent with that determined from *post-mortem* TEM imaging of the tip apex by fitting the traced tip profile to a circle (Fig. S-2) of 10.2±0.6 nm; TEM imaging was not possible for Tip 2. Using the tip radii (from TEM for Tip 1 and DMT for Tip 2) and the materials' elastic constants (E = 78 GPa and ν = 0.44 for gold [30], and E = 55.6 GPa and ν = 0.16 for SiO_2 [31]), the contact radii were calculated to be 1.2±0.2 nm

and 0.8±0.5 nm for Tips 1 and 2, respectively. From the slope of the friction trace during the "stick" phase of scanning, the effective lateral stiffness was determined to be 5.4±0.7 N/m and 5.5±0.9 N/m for Tips 1 and 2, respectively.

Figure 1 shows the mean experimental friction *vs*. scanning speed for both tips, with an inset showing a friction loop acquired at a scanning speed of 5.8 μm/s. Single atomic stick-slip events were resolved up to speeds ~10 μm/s, after which the number of data points per event were insufficient. For both data sets, the expected near-logarithmic increase in friction with speed is observed from the minimum scanning speed (~1.7 nm/s), until a plateau occurs at ~1-10 μm/s. The data was fit to the PTT model [9,13] using the equation:

$$\frac{1}{\beta k_B T}(F_c - F_L)^{3/2} = \ln\frac{v_0}{v} - \frac{1}{2}\ln\left(1 - \frac{F_L}{F_c}\right) \quad (1)$$

where F_L is the mean static friction force, v is the scanning speed, T is the temperature, k_B is Boltzmann's constant, F_c is the mean static friction force at zero kelvin, β is a parameter related to the shape of the lateral potential profile that governs the rate of increase of friction with speed at low speeds, and v_0 is a characteristic speed given by $v_0 = (2f_0\beta k_B T)/\left(3k_{tot}\sqrt{F_c}\right)$, where f_0 is the characteristic slip attempt frequency, and k_{tot} the total lateral stiffness of the system [9,32,33]. For a sinusoidal potential with periodicity a and a barrier height E_0: $F_c = \pi E_0/a$ and $\beta = 3\pi\sqrt{F_c}/\left(2\sqrt{2}a\right)$.

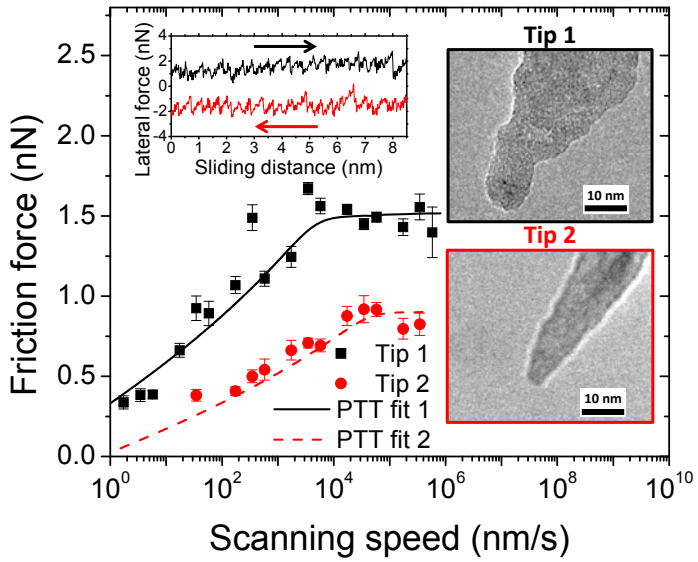

Figure 1: Friction force *vs.* scanning speed for Tip 1 (black squares) and 2 (red circles). The solid line (Tip 1) and dashed line (Tip 2) are fits of the PTT model to the data, which yield, for Tip 1: F_c= 1.5±0.2 nN, β = (4.8 ± 2.0)×10^5 $N^{3/2}$/J, and f_0 = 108±42 kHz; and for Tip 2: F_c = 0.9±0.2 nN, β = (2.5±0.3)×10^5 $N^{3/2}$/J, and f_0 = 700±200 kHz. The normal applied force is 0.0±0.2 nN in both data sets. Error bars represent the standard deviation in the calculated mean friction force. Right insets are *pre-mortem* TEM images of the tips used for data acquisition. Top-left inset shows a friction loop acquired with Tip 1 at ~5.8 μm/s; an atomic stick-slip pattern can be clearly resolved corresponding to scanning along the [110] direction. Arrows indicate the scan direction.

The three parameters, β, f_0, and F_c, were obtained by fitting the data to the PTT model. F_c was determined first as an average of the data points in the plateau. Then β and f_0 were fit to the data at all scanning speeds with their resulting values (Fig. 1, caption) differing between the two tips by factors of 1.9 and 6.5 respectively. These are reasonable given the differences in the two tip sizes and shapes; a more complete discussion is provided in the SM [17].

Complementary simulations consisted of the apex of an amorphous SiO_2 AFM tip scanning over a Au(111) surface with dimensions of 10×10×5 nm^3 (length × width × thickness). The key achievement here is the implementation of PRD, necessary to increase the duration of the simulations thereby decreasing the scanning speeds [34,35], with a 0.1 nm transition criterion and 10 ps between transition checks. Speeds as low as 25 μm/s were achieved. The PRD method was optimized by the use of a truncated cone-shaped tip as it was highly stable, minimizing the number of atomic transitions not related to slips. The effective lateral contact stiffness of the

system was set to 5.38 N/m, within the error of both experimental values. A Langevin thermostat was applied to unconstrained atoms in the system, which was maintained at a temperature of 300 K. Additional model details are provided in the SM [17].

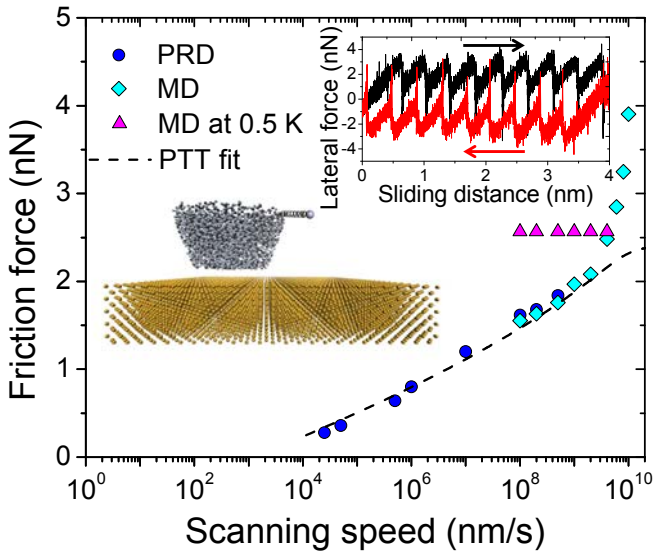

Figure 2: Friction force as a function of scanning speed from MD at 300 K (cyan diamonds) and 0.5 K (purple triangles), and PRD (blue circles) at 300 K. Dashed lines indicate fits of the PRD data to the PTT model using a value of F_c of 2.56±0.02 nN from the simulations run at 0.5 K, yielding β=(2.9±0.2)×10^5 N$^{3/2}$/J and f_0=120±30 GHz. Left inset: model of the SiO_2 tip and the Au(111) substrate. Top right inset: a friction loop showing clear atomic stick-slip along the [100] direction. Arrows indicate the scan direction.

The simulation-predicted mean friction force is shown in Figure 2. Significantly, the slowest scanning speed obtained from PRD simulations (25 μm/s) is smaller than the fastest speed of experiments (~580 μm/s). Overlapping datapoints at 0.1, 0.2 and 0.5 m/s from MD and PRD validate the PRD simluations. MD simulations were run at 0.5 K to mimic sliding friction without thermal activation; the resulting constant friction force plateau at 2.56±0.02 nN was used as F_c in the PTT model fit. Above scanning speeds of 4 m/s, friction increased rapidly with speed, deviating from the predicted plateau. The unphysically high friction at high speeds is consistent with previous observations, although no physical explantation was provided [8]. The present simluations reveal that it is associated with surface wear, quantified empirically as the the root mean square surface roughness, which was observed to increase dramatically at these speeds (Figure S-3). The high speed data was excluded from subsequent analyses, enabling isolation of

friction from wear and subsequent fits of the data to the wearless PTT model. Fitting the simulation data up to 1 m/s then yields $\beta = (2.9\pm0.2)\times10^5$ N$^{3/2}$/J, and $f_0 = 120\pm30$ GHz.

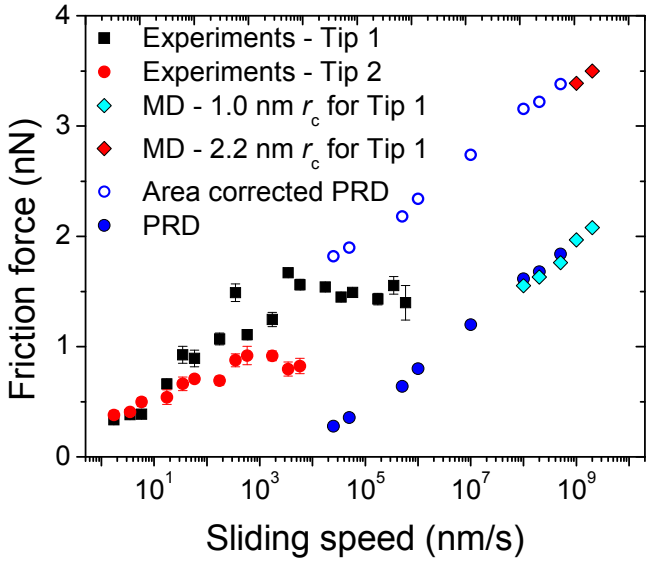

Figure 3: MD (cyan and red solid diamonds), PRD (blue solid circles), and experimental results from Tip 1 (black squares) and Tip 2 (red solid circles) plotted together. MD predictions are reported for 1.0 nm (cyan diamonds) and 2.2 nm (red diamonds) contact radii, r_c, where the latter is consistent with an extrapolation of the low-speed increasing friction trend observed in the experiments for Tip 1. The relationship between F_c and contact size is also used to extrapolate the PRD data to a 2.2 nm contact radius (blue hollow circles).

To better compare experiment and simulation, the AFM data from Tip 1 (black squares) and the MD/PRD data (diamonds and blue circles) are plotted together in Figure 3. This clearly shows that while the speed gap between simulations and experiment has been closed, a significant difference exists despite the optimally matched conditions. Comparison of the fit values obtained for β, F_c, and f_0 provides clues to the origins of this difference. The β values are reasonably consistent across simulation and experiments (2.9×10^5 N$^{3/2}$/J from simulation, and 4.8×10^5 N$^{3/2}$/J and 2.5×10^5 N$^{3/2}$/J from experiments). The magnitude of F_c derived from simulation (2.56 nN) was somewhat larger than the two experimental values (0.85±0.18 and 1.5±0.2 nN), but was on the same order of magnitude. However, the value of f_0 from simulation (120±30 GHz) differed by orders of magnitude from those from the experiments (108±42 kHz and 700±200 kHz). The remainder of this manuscript examines the root causes of the differences in F_c and f_0, which may explain the difference in the predicted and measured friction.

The discrepancy in F_c may have three origins: differences in tip shape, scanning direction, and contact area. First, a truncated cone-shaped model tip was used to optimize the PRD simulations; this differs from the hemispherical experimental shape indicated by TEM images (Figure 1, inset). The influence of tip geometry was investigated by simulating a hemispherical tip with the same approximate contact radius as that of the truncated cone; these simulations were performed only at fast scanning speeds (*i.e.* using MD, not PRD). The change to a hemispherical model tip increased friction only slightly (~6%) (Fig. S-4), an amount within the uncertainty of the contact mechanics calculations, indicating that geometry cannot explain the experiment-simulation difference. Second, the scanning direction was [110] in the experiments and [100] in the simulations. However, MD simulations run over a range of scanning directions produced only a ~4% change in mean friction force (Fig. S-5). Therefore, scanning direction was also unlikely to contribute to the discrepancy. Finally, the effect of contact area was evaluated. Recall that the simulation contact area was designed to match a value estimated from experiments, where that estimate was based on a continuum model, a limitation imposed by being unable to directly measure contact area experimentally [29]. To test the sensitivity of F_c to contact area, simulations with truncated cone-shaped tips having different circular contact radii were conducted. Friction increased linearly with contact area (Fig. S-6), consistent with previous theoretical [15] and experimental observations [36,37]. The linear relationship between friction and contact area suggested that increasing the model simulation contact radius from 1.0 nm to 2.2 nm, which also increases the mass of the tip from 5.79×10^{-23} kg to 9.70×10^{-23} kg, should result in good agreement between simulation and the low-speed friction trend from experiment (Figure 3: MD simulation data, red diamonds; extrapolated PRD data, hollow blue circles). This contact radius (2.2 nm) is consistent with the experimental estimation, and certainly feasible given the limitations of using a continuum model to describe nanoscale contact [38,39] and the large error associated with determining the tip radius. This suggests that the contact area may contribute to the observed difference in friction between experiment and simulation. However, such a shift will not resolve the complete disagreement in the onset speed of the plateau.

The experiment-simulation discrepancy can only be fully resolved by addressing the difference in attempt frequency, f_0. Mass (inertia) may be one cause of this difference, as discussed previously [8]. However, unlike the previous study, here no extrapolation of the data to

fit the PTT model was necessary. Furthermore, the possibility of effects due to surface contamination can be excluded since the experiments were performed in UHV. We therefore can compare the results with confidence. In analyzing the tip masses, the tip apex in MD/PRD simulation is only comprised of a few thousand atoms, significantly smaller than the AFM tip or the cantilever, both of which exhibit thermal vibrations that can produce slip attempts. For a harmonic system, the attempt frequency will be related to the structure's effective mass, m, by $f_0 = \frac{1}{2\pi}\sqrt{\frac{k}{m}}$, where k is the spring stiffness. This expression, with the fit values of f_0 from experiment and simulation and the known simulation tip mass, predicts an effective experimental tip mass of m_{exp}~10^{-11} kg, corresponding to a volume of ~4×10^{-15} m^3 (assuming a density of 2.6 g/cm^3 [40]). While it is not exactly known how much of the tip actually contributes to thermally activated friction, the calculated volume is consistent with that of a real AFM tip, estimated to be ~7×10^{-16} m^3 based on the TEM tip images and the use of a method of disks from the tip profile [41]. This range of masses cannot be directly tested using MD simulations given the size-scale limitations of the model. However, simulations of tips scanning at 1 m/s with artificially increased atom masses showed that friction increased with mass (Fig. S-7), consistent with our numerical solutions of the PTT model (higher mass reduces f_0; fewer slip attempts per unit time lead to higher mean friction, similar to the effect of scanning faster). Thus, the small model tip mass provides one explanation for the difference between simulation and experiment.

However, within the range of contact areas, tip masses, and scanning speeds explored in the simulations, the experimentally observed friction plateau is not reproduced. Physically, the plateau represents attaining a high enough scanning speed that available vibrations of the atoms at the end of the tip apex no longer have enough time assist in overcoming the local interfacial potential energy barriers [42]. In the PTT model, only those thermal vibrations of the tip apex are considered. However, other thermal noise sources, such as thermally induced vibrations of the cantilever, or athermal instrument noise, such as mechanical vibrations of the AFM apparatus and electronic 60 Hz noise, are not included despite the fact that they too can lower the activation barrier to slip by adding energy into the contact [42,43]. Both athermal and thermal noise sources are inherent in every experiment, but not fully captured in simulations. By applying the master equation method [44], the influence of both noise sources can be captured simultaneously via numerical modeling. In this approach, both noise sources are specified in the model, with the

magnitude of the athermal noise vibration to be modeled determined by calibrating its amplitude in the experiment with respect to the amplitude of the cantilever's thermal noise (as determined in a power spectrum of cantilever signal). This analysis indicates that two transition points can occur: a plateau-like reduction in slope at low speed determined by low frequency instrument noise, and a plateau at high speed due to higher frequency thermal noise [43] (Fig. S-8). The master equation method was applied (details in SM [17]) assuming thermal or athermal excited vibration of the cantilever at 200 kHz and an amplitude of 0.20 nm. This amplitude corresponds to an effective temperature of 1800 K based on the equipartition theorem [45], thus, the noise observed in the experiment is likely a combination of the thermal noise from the AFM cantilever oscillating at its first lateral resonance and athermal noise associated with the mechanical vibrations of the AFM apparatus. This modeling is the only current mechanism by which the low-speed friction plateau observed in experiments and the high-speed friction plateau observed in simulations can be linked.

In summary, the speed dependence of atomic stick-slip friction between silica AFM tip apexes and atomically-flat gold surfaces has been studied using optimally-matched AFM experiments and MD simulations with overlapping scanning speeds. For both experiments and simulations, the friction *vs*. scanning speed trend matches that predicted for thermally activated slip, but the magnitude of forces and the onset speed of the friction plateau disagree. Analysis of the PTT parameters corresponding to the simulation and experiments indicates that the interfacial potential shape parameters match well, small differences in the mean athermal friction force may contribute, but vastly different attempt frequencies are at play. The magnitude of the friction forces can be explained by differences in contact area, but the onset of the plateau requires justifying the discrepancy in the attempt frequency. This can be attributed to noise from the thermal vibrations of the cantilever or other athermal noise sources within the instrumentation.

This study thus bridges the gap between atomic scale friction mechanisms and those observed for real mechanical systems by observing atomic stick-slip over nine orders of magnitude. Across this range, stick-slip is observed to follow the PTT model: the tip resides in and then escapes from local potential energy minima, due to the applied shear force assisted by vibrations. This validates using the rich array of data available from MD simulations to interpret AFM experimental results.

Acknowledgments

The authors acknowledge the Nanoscale Characterization Facility at the University of Pennsylvania for use of instrumentation, technical support from Dr. Q. Li, Q. Tam, J. Hilbert, J. Lefever, and H. Zhu, and financial support from NSF/ENG grant no. CMMI-1362565, CMMI-1068552, and CMMI-1401164. P.E. acknowledges financial support from a Natural Sciences and Engineering Research Council (NSERC) of Canada Postdoctoral Fellowship (PDF). Y.D. acknowledges support from startup funds of the University of Akron.

[1] A. Socoliuc, E. Gnecco, S. Maier, O. Pfeiffer, A. Baratoff, R. Bennewitz, and E. Meyer, Science **313**, 207 (2006).
[2] S. Y. Krylov and J. W. M. Frenken, Physica Status Solidi (b) **251**, 711 (2014).
[3] S. Morita, S. Fujisawa, and Y. Sugawara, Surface Science Reports **23**, 1 (1996).
[4] C. M. Mate, G. M. McClelland, R. Erlandsson, and S. Chiang, Physical Review Letters **59**, 1942 (1987).
[5] L. Prandtl, Zeitschrift für Angewandte Mathematik und Mechanik **8**, 85 (1928).
[6] G. A. Tomlinson, Philosophical Magazine **7**, 905 (1929).
[7] S. Medyanik, W. Liu, I.-H. Sung, and R. W. Carpick, Physical Review Letters **97** (2006).
[8] Q. Li, Y. Dong, D. Perez, A. Martini, and R. W. Carpick, Physical Review Letters **106**, 126101 (2011).
[9] E. Riedo, E. Gnecco, R. Bennewitz, E. Meyer, and H. Brune, Physical Review Letters **91**, 84502 (2003).
[10] A. Schirmeisen, L. Jansen, H. Hölscher, and H. Fuchs, Applied Physics Letters **88**, 123108 (2006).
[11] J. Chen, I. Ratera, J. Park, and M. Salmeron, Physical Review Letters **96** (2006).
[12] N. S. Tambe and B. Bhushan, Journal of Physics D: Applied Physics **38**, 764 (2005).
[13] Y. Sang, M. Dubé, and M. Grant, Physical Review Letters **87** (2001).
[14] Y. Dong, Q. Li, and A. Martini, Journal of Vacuum Science & Technology A: Vacuum, Surfaces, and Films **31**, 030801 (2013).
[15] I. Szlufarska, M. Chandross, and R. W. Carpick, Journal of Physics D: Applied Physics **41**, 123001 (2008).
[16] C. Nogues and M. Wanunu, Surface Science **573**, L383 (2004).
[17] See Supplemental Material [url], which includes Refs. [18-25].
[18] J. Tersoff, Physical Review B **38**, 9902 (1988).
[19] M. S. Daw and M. I. Baskes, Physical Review Letters **50**, 1285 (1983).
[20] M. S. Daw and M. I. Baskes, Physical Review B **29**, 6443 (1984).
[21] R. W. Carpick, D. F. Ogletree, and M. Salmeron, Journal of Colloid and Interface Science **211**, 395 (1999).
[22] K. Johnson, K. Kendall, and A. Roberts, Proceedings of the Royal Society of London. A. Mathematical and Physical Sciences **324**, 301 (1971).
[23] Y. Zhu, Q. Qin, Y. Gu, and Z. Wang, Nanoscale Research Letters **5**, 291 (2009).
[24] H. A. Lorentz, Annalen der Physik **248**, 127 (1881).
[25] D. Berthelot, Compt. Rendus **126**, 1703 (1898).

[26] Q. Li, Y. Dong, A. Martini, and R. W. Carpick, Tribology Letters, 1 (2011).
[27] E. Meyer, H. J. Hug, and R. Bennewitz, *Scanning probe microscopy: the lab on a tip;* (Springer Verlag, 2004).
[28] P. Egberts, Z. Ye, X.-Z. Liu, Y. Dong, A. Martini, and R. W. Carpick, Physical Review B **88** (2013).
[29] B. Derjaguin, V. Müller, and Y. P. Toporov, Journal of Colloid and Interface Science **53**, 314 (1975).
[30] J. D. Kiely and J. E. Houston, Physical Review B **57**, 12588 (1998).
[31] C.-L. Dai and Y.-M. Chang, Materials Letters **61**, 3089 (2007).
[32] E. Gnecco, R. Bennewitz, T. Gyalog, C. Loppacher, M. Bammerlin, E. Meyer, and H. Güntherodt, Physical Review Letters **84**, 1172 (2000).
[33] S. J. Manzi, W. T. Tysoe, and O. J. Furlong, Tribology Letters **55**, 363 (2014).
[34] A. F. Voter, Physical Review B **57**, R13985 (1998).
[35] B. P. Uberuaga, S. J. Stuart, and A. F. Voter, Physical Review B **75**, 014301 (2007).
[36] M. Enachescu, R. J. A. van den Oetelaar, R. W. Carpick, D. F. Ogletree, C. F. J. Flipse, and M. Salmeron, Tribology Letters **7**, 73 (1999).
[37] M. A. Lantz, S. J. O'Shea, M. E. Welland, and K. L. Johnson, Physical Review B **55**, 10776 (1997).
[38] Y. Mo, K. T. Turner, and I. Szlufarska, Nature **457**, 1116 (2009).
[39] B. Luan and M. O. Robbins, Nature **435**, 929 (2005).
[40] D. R. Lide, *CRC Handbook of Chemistry and Physics* (CRC press, 2004), 85th edn.
[41] T. D. B. Jacobs and R. W. Carpick, Nature Nanotechnology **8**, 108 (2013).
[42] A. Labuda, M. Lysy, W. Paul, Y. Miyahara, P. Grütter, R. Bennewitz, and M. Sutton, Physical Review E **86** (2012).
[43] Y. Dong, H. Gao, A. Martini, and P. Egberts, Physical Review E **90**, 012125 (2014).
[44] D. Perez, Y. Dong, A. Martini, and A. F. Voter, Physical Review B **81**, 245415 (2010).
[45] J. L. Hutter and J. Bechhoefer, Review of Scientific Instruments **64**, 1868 (1993).